JOURNAL OF STRUCTURAL BIOLOGY **119,** 149–157 (1997)
ARTICLE NO. SB973878

Structural Changes in Native Membrane Proteins Monitored at Subnanometer Resolution with the Atomic Force Microscope: A Review

Daniel J. Müller

Biozentrum, M. E. Müller Institute for Microscopy, Klingelbergstrasse 70, CH-4056 Basel, Switzerland; and IBI-2: Structural Biology, Forschungszentrum Jülich, D-52425 Jülich, Germany

Cora-Ann Schoenenberger

Biozentrum, M. E. Müller Institute for Microscopy, Klingelbergstrasse 70, CH-4056 Basel, Switzerland

Frank Schabert

Institute of Physics, Humboldt University Berlin, Unter den Linden 6, D-10115 Berlin, Germany

and

Andreas Engel

Biozentrum, M. E. Müller Institute for Microscopy, Klingelbergstrasse 70, CH-4056 Basel, Switzerland

Received February 11, 1997, and in revised form April 17, 1997

Three membrane proteins, OmpF porin from *Escherichia coli*, bacteriorhodopsin from *Halobacterium salinarium*, and the hexagonally packed intermediate (HPI) layer from *Deinoccocus radiodurans*, were investigated with the atomic force microscope in buffer solution. A resolution of up to 0.8 nm allowed structural differences of individual proteins to be detected. OmpF porin exhibits different static conformations on the outer surface, which possibly represent the two conductive states of the ion channels. Reversible structural changes in the cytoplasmic surface of purple membrane have been induced by changing the force applied to the scanning stylus: doughnut-shaped bacteriorhodopsin trimers transformed into a structure with three pronounced protrusions when the force was reduced from 300 to 100 pN. Furthermore, individual pores of the inner surface of the HPI layer were observed to switch from an "open" to a "closed" state. Together, the structural changes in proteins monitored under physiological conditions suggest that direct observation of function-related conformational changes of biomolecules with the atomic force microscope is feasible.

INTRODUCTION

Shortly after the invention of the scanning tunneling microscope (STM; Binnig *et al.*, 1982) and the atomic force microscope (AFM; Binnig *et al.*, 1986), the potential of these new microscopical techniques for biological applications was recognized (Drake *et al.*, 1989). Since atomic resolution has been achieved with the STM (Binnig *et al.*, 1982; Sonnenfeld and Hansma, 1986) and the AFM (Binnig *et al.*, 1987; Ohnesorge and Binnig, 1993), scanning probe microscopes have been considered competitors to conventional methods for structural investigations, such as electron microscopy, NMR, and X-ray scattering. Since the physical basis of STM is the tunneling current between the stylus and the sample, the information contained in an STM image represents a combination of the topography and the electron density of the sample surface. Unfortunately, most biological macromolecules are nonconducting and cannot be imaged with the STM unless coated with a conducting layer, such as PtIrC (Amrein, 1989; Stemmer *et al.*, 1991; Knapp *et al.*, 1995) or, as recently shown, with a few monolayers of water (Guckenberger *et al.*, 1994; Maaloum *et al.*, 1994). The physical basis of the AFM lies in the various forces

1047-8477/97 $25.00

interacting between stylus and sample. AFM images either reflect surface topographies sensed with a distinct force (constant force mode) or represent the deflection of the cantilever while the sample is scanned at constant height. One of the big advantages of the AFM is its ability to monitor native insulating or conducting specimens, which can be investigated in air and vacuum or, most enticing to biologists, in aqueous solution. Both techniques, STM and AFM, can provide structural information on surfaces. Complementary structural information on the volume of a macromolecule can be obtained only by electron microscopy, NMR, and X-ray scattering. Without this information, it is often not possible to interpret the surface topography of a biological macromolecule and its conformational changes.

As result of the high signal-to-noise ratio, the AFM allows monitoring of submolecular details of proteins under physiological conditions (Hoh *et al.*, 1991, 1993; Karrasch *et al.*, 1993, 1994; Yang *et al.*, 1993; Schabert and Engel, 1994; Mou *et al.*, 1996; Müller *et al.*, 1995b). In this review, we report on three protein arrays, OmpF porin, bacteriorhodopsin, and the hexagonally packed intermediate (HPI) layer, all of which have been imaged in aqueous solution at submolecular resolution with the AFM. The two conformations observed on the extracellular surface of OmpF porin (Schabert *et al.*, 1995), the dynamic process of the reversible, force-induced conformational change in bacteriorhodopsin (Müller *et al.*, 1995a), and the time-dependent conformational changes in individual pores in the HPI layer (Müller *et al.*, 1996a) foster the hope that function-related conformational changes in proteins induced by a physiological signal can be directly monitored with the AFM.

CONFORMATIONAL DIFFERENCES MONITORED WITH THE AFM

Static Conformational Differences

OmpF porin represents a channel forming protein in the outer membrane of the *Escherichia coli* cell. It facilitates the diffusion of hydrophilic molecules ($<$600 M_r) in both directions across the membrane. OmpF porin is weakly cation selective and exhibits a voltage (Lakey, 1987) as well a pH sensitivity (Todt *et al.*, 1992). The monomers consisting of 340 amino acids (M_r 37 200; Rosenbusch, 1974) are arranged into a trimeric structure which has been solved by X-ray crystallography (Cowan *et al.*, 1992). Each monomer comprises a barrel made of 16 antiparallel β-strands forming a channel through which nutrients diffuse (Cowan *et al.*, 1992). Access to the channel from the extracellular environment is controlled by one interstrand loop that folds into the pore (Schulz, 1993).

For their assembly into 2D crystals, OmpF porin trimers from *E. coli* B^e strain (Hoenger *et al.*, 1993) were solubilized in octylpolyoxyethylene and mixed with solubilized dimyristoyl phosphatidylcholine (99% purity, Sigma Chemical Co., St. Louis, MO) at a lipid-to-protein ratio (w/w) of 0.2 and a protein concentration of 1 mg/ml. The mixture was reconstituted in a temperature-controlled dialysis device (Jap *et al.*, 1992). The 2D crystal containing solution (1 mg protein/ml) was diluted to a concentration of 5 μg/ml in the adsorption buffer (10 m*M* NaH_2PO_4, 140 m*M* NaCl, 2.5 m*M* $MgCl_2$, pH 7.4). A drop of this solution was deposited onto freshly cleaved mica. After an adsorption time of 10 min, the sample was gently rinsed with adsorption buffer to remove membrane sheets that were not firmly attached to the support.

When 2D crystals of OmpF porin were immobilized on freshly cleaved mica, the surface topography could be reproducibly monitored at high resolution (Schabert and Engel, 1994). Figure 1a shows the topography of the periplasmic surface of OmpF porin. The relatively smooth surface, which protrudes less than 0.5 nm from the lipid bilayer, was imaged at a lateral resolution of 0.8 nm determined by Fourier ring correlation function (Schabert and Engel, 1994). The periplasmic surface exhibited struc-

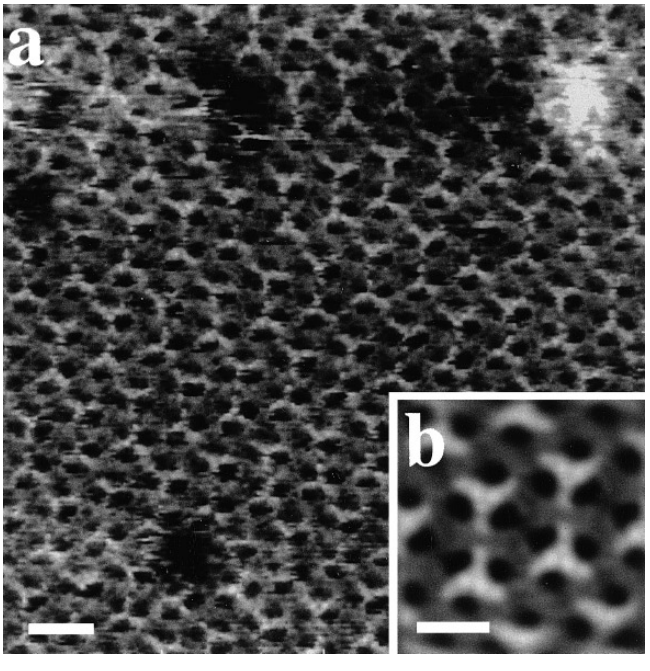

FIG. 1. Periplasmic surface of a two-dimensional OmpF porin crystal. (a) The topography displays the rectangular arrangement of the porin trimers. Lattice defects such as disordering and point defects are distinct. (b) Correlation average of (a). The image was recorded in contact mode and buffer solution. Applied force ≈200 pN. Scale bars, 10 nm (a) and 5 nm (b). The full gray level range corresponds to 3 and 1.5 nm in (a) and (b), respectively.

tural details of the porin trimers comprising three channels that were separated by 1.2-nm-thick walls. As displayed in the correlation average (Fig. 1b), the channels showed an elliptical cross section (a = 3.4 nm, b = 2.0 nm). Between the three protrusions close to the threefold axis, a small depression was evident. Assuming a lateral resolution of 1 nm and a vertical resolution of 0.1 nm, the observed topography was in excellent agreement with the atomic structure (Schabert *et al.*, 1995).

The surface loops that connect the β-strands on the periplasmic side are very short and contain polar residues in hydrogen-bonded reverse turns. In comparison, the extracellular surface (Fig. 2a) exhibits longer external loops. They are rich in charged amino acids and fold into complex structures, including three short α-helices (Cowan *et al.*, 1992). The longer loops resulted in trimeric corrugations that protruded 1.1 ± 0.2 nm above the lipid bilayer (Schabert *et al.*, 1995). Because of the extended roughness of the extracellular surface, the lateral resolution of approximately 1.3 nm was not as high as that achieved on the periplasmic surface. Furthermore, the extracellular surface showed an increased flexibility, and high-resolution images required imaging at forces of 100 pN (1 piconewton = 10^{-12} N). Occasionally, it appeared that the domains of the extracellular surface exhibited a different conformation (Fig. 2c). The image shown in Fig. 2c was recorded with the same stylus as that used for Fig. 2a. Thus, it is highly unlikely that the observed structural differences are due to tip artifacts. The correlation-averaged and threefold-symmetrized topography allowed us to visualize the differences in both conformations in more detail (Figs. 2b and 2d). From the averages it became clear that the extracellular domains of the conformation in Fig. 2d were shifted toward the center of the trimer by about 0.5 nm. This suggests that OmpF porin exhibits two states, an "open" conformation (Figs. 2a and 2b) and a "closed" conformation (Figs. 2c and 2d; Schabert *et al.*, 1995). However, to correlate the different conformations of OmpF porin directly with its function, conformational changes must be induced and subsequently monitored.

Reversible Force-Induced Conformational Changes

Bacteriorhodopsin is a light-driven proton pump that absorbs light (λ_{max} = 560 nm) and builds up an electrochemical potential across the inner cell membrane of the archaebacteria *Halobacterium salinarium*. Naturally, bacteriorhodopsin molecules are arranged in trimers which form a 2D trigonal lattice (a = 6.2 nm), the so-called purple membrane. Bacteriorhodopsin consists of seven transmembrane α-helices (Henderson *et al.*, 1990) surrounding the photoreactive retinal (Jubb *et al.*, 1984). Upon exposure to light the chromophore isomerizes from all-*trans* to the 13-*cis* isoform, which leads to a proton translocation assisted by the movement of the transmembrane α-helices (Dencher *et al.*, 1989; Subramaniam *et al.*, 1993). A similar arrangement of seven α-helical membrane spanning segments has been observed for halorhodopsin (Havelka *et al.*, 1993) and rhodopsin (Schertler *et al.*, 1993). This feature also appears to represent a common motif of the G-protein-

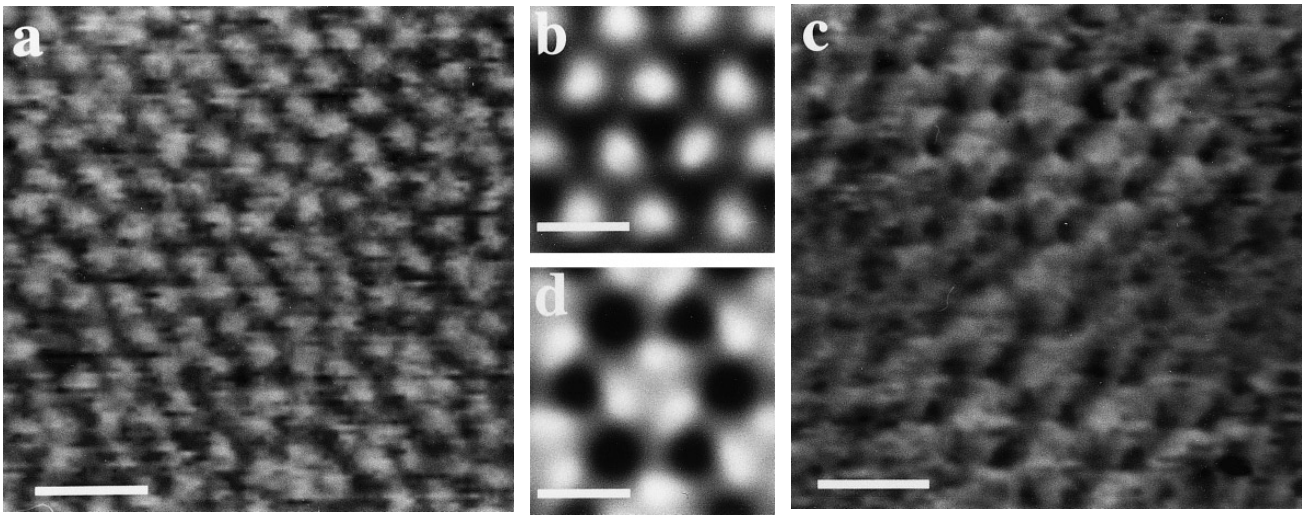

FIG. 2. Two conformations of the extracellular surface of hexagonally arranged porin. (a) The "open" conformation of the OmpF porin trimer is visible in the unprocessed image and more clearly in the averaged topography (b). (c) The "closed" conformation of the porin trimer was imaged with the same stylus. The protrusions of the trimer are more compact. (d) Average of (c). Images were recorded in contact mode and buffer solution, applying a force of 100 pN. Scale bars, 10 nm (a, c) and 5 nm (b, d). The full gray level range corresponds to 4 and 2 nm in (a, c) and (b, d), respectively.

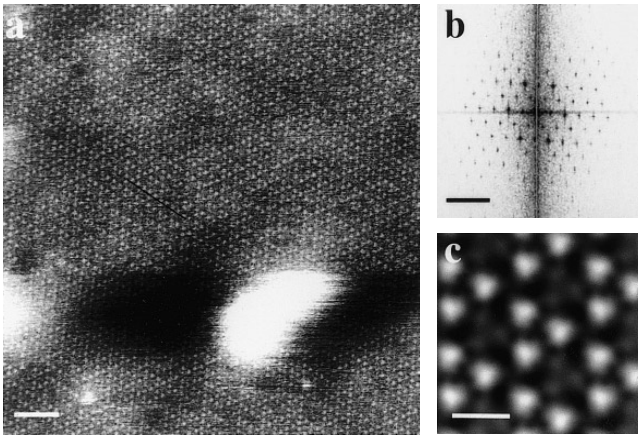

FIG. 3. Extracellular surface of purple membrane. (a) High-resolution topography imaged in contact mode. (b) Diffraction pattern of (a). (c) Correlation-averaged and threefold-symmetrized topography. Image was recorded in buffer solution, loading force ≈100 pN. Scale bars, 20 nm (a), 2 nm^{-1} (b), and 4 nm (c). The full gray level range corresponds to 1 and 0.5 nm in (a) and (c), respectively.

coupled receptor family (Baldwin, 1993). Purple membrane consists of 75% (w/w) bacteriorhodopsin and 25% lipids (Kates *et al.*, 1982) which play a specific role in the 2D crystal lattice. The atomic model of bacteriorhodopsin has been derived from electron crystallography to a resolution of 3.5 Å (Grigorieff *et al.*, 1996). The most disordered part of the structure consists of loops connecting the membrane spanning α-helices. Here, topographies recorded at subnanometer resolution with the AFM (Müller *et al.*, 1995a,b) can provide useful information. After identification of the cytoplasmic surface by *in situ* labeling with antibodies directed against the C-terminal end, the purple membrane surfaces were imaged with the AFM (Müller *et al.*, 1996b).

Purple membranes of *H. salinarium* strain ET1001 were isolated as described by Oesterhelt and Stoeckenius (1974). The membranes were frozen and stored at −70°C. Thawed samples were kept at 4°C. A stock solution (10 mg/ml protein) in distilled water was diluted to 10 µg/ml in 150 m*M* KCl, 10 m*M* Tris–HCl, pH 8, prior to adsorption to freshly cleaved mica. After an adsorption time of 10 min, the sample was gently washed and then imaged in the same buffer.

The topography of native purple membrane was imaged at subnanometer resolution (Figs. 3 and 4) with the AFM (Müller *et al.*, 1995a,b and 1996b). On its extracellular surface (Fig. 3a), purple membrane exhibited a major and a minor trimeric protrusion per bacteriorhodopsin trimer. The average height above the lipid bilayer was about 0.2 ± 0.02 nm. It is conceivable that the carbohydrates of the glycolipids, which represent the majority of lipids in the extracellular leaflet of the bilayer (Henderson *et al.*, 1978), prevent the stylus from reaching the lipid head groups. The power spectrum (Fig. 3b) exhibited characteristic strong second-order spots, while higher orders extended all the way out to the Nyquist cutoff at $(0.7\ nm)^{-1}$. After threefold symmetrization of the correlation averages (Fig. 3c), both tripartite domains arranged on equilateral triangles were distinct. While the major domains (height 0.2 nm) were separated by 2.9 nm, the three minor domains (height 0.08 nm) were 1.9 nm apart.

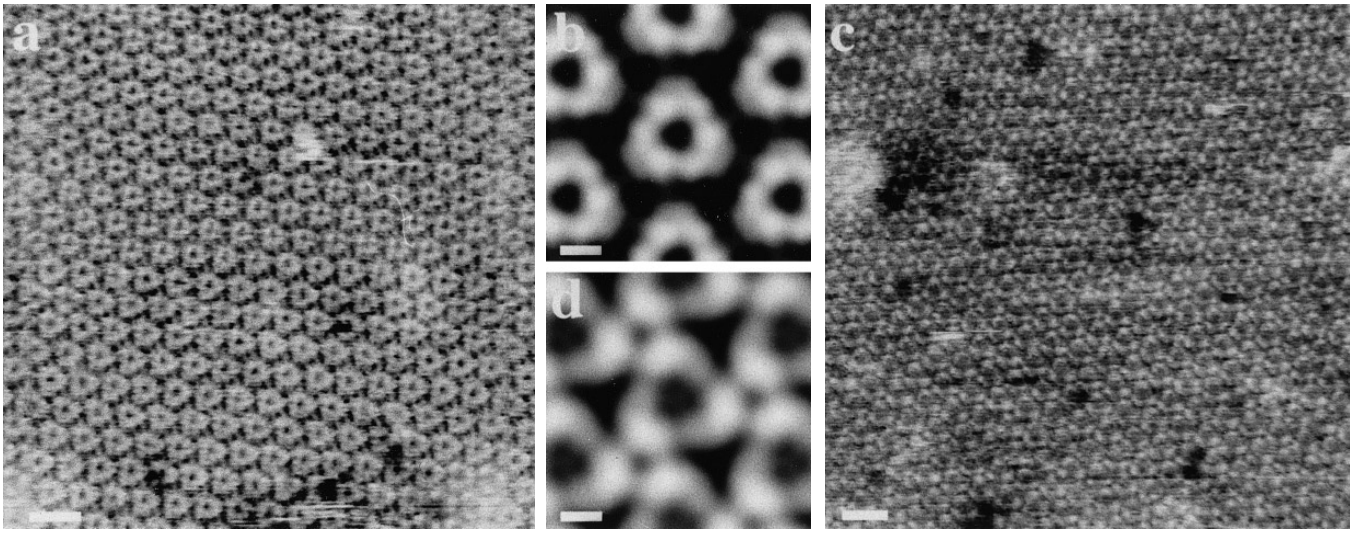

FIG. 4. Two conformations of the cytoplasmic surface of purple membrane. (a) High-resolution topography recorded at ≈300 pN. (b) Threefold-symmetrized correlation average of (a). (c) Topography of the bacteriorhodopsin trimers scanned with a force of ≈150 pN. (d) Average of (c). Images were recorded in contact mode and buffer solution. Scale bars, 10 nm (a, c) and 2 nm (b, d). The full gray level range corresponds to 2 and 1 nm in (a, c) and (b, d), respectively.

Two different conformations have been observed on the cytoplasmic surface of purple membrane (Figs. 4a and 4c). When imaged at about 250–500 pN, the bacteriorhodopsin trimers revealed a distinct doughnut-like shape (Fig. 4a). Although the appearance of the doughnuts varied considerably, their tripartite morphology was consistent. After symmetrization of 760 correlation-averaged unit cells (Fig. 4b), the tripartite morphology of the doughnuts was pronounced and the trimers appeared to be connected by fibrous arms. The two domains per bacteriorhodopsin monomer were 1.45 ± 0.1 nm apart, arranged on circles with radii of 1.47 ± 0.1 and 1.67 ± 0.1 nm, respectively. As a result, different distances between inner domains (2.65 ± 0.1 nm) and outer domains (2.89 ± 0.1 nm) dominated the topography. The corrugation amplitude of averaged and symmetrized unit cells was 0.4 ± 0.03 nm. It was possible to record the cytoplasmic surface in another conformation (Fig. 4c) when scanning forces between 100 and 150 pN were applied. Specifically, the bacteriorhodopsin trimers revealed a more tripartite topography with three major protrusions at the periphery of the doughnuts (Fig. 4d). The intertrimeric distances of the correlation-averaged and symmetrized topography corresponded to about 2.2 nm, while their height above the lipid bilayer was 0.6 ± 0.02 nm.

Bacteriorhodopsin molecules can undergo conformational changes in response to alterations in the force applied by the stylus. The different conformations of the cytoplasmic surface (Fig. 4) can be recorded in a single topography when the force is decreased from 300 to 100 pN during imaging (Fig. 5; Müller *et al.*, 1995a). The conformational change is fully reversible and can be repeated on the same membrane area over hours of continuous scanning. Recorded at 300 pN, the bacteriorhodopsin trimers showed a doughnut-shaped topography (Figs. 4a and 4b). Successive reduction of the force was associated with structural changes in individual bacteriorhodopsin molecules. Imaged at minimum forces of approximately 100 pN, the topography of the bacteriorhodopsin trimers changed to more pronounced trimeric

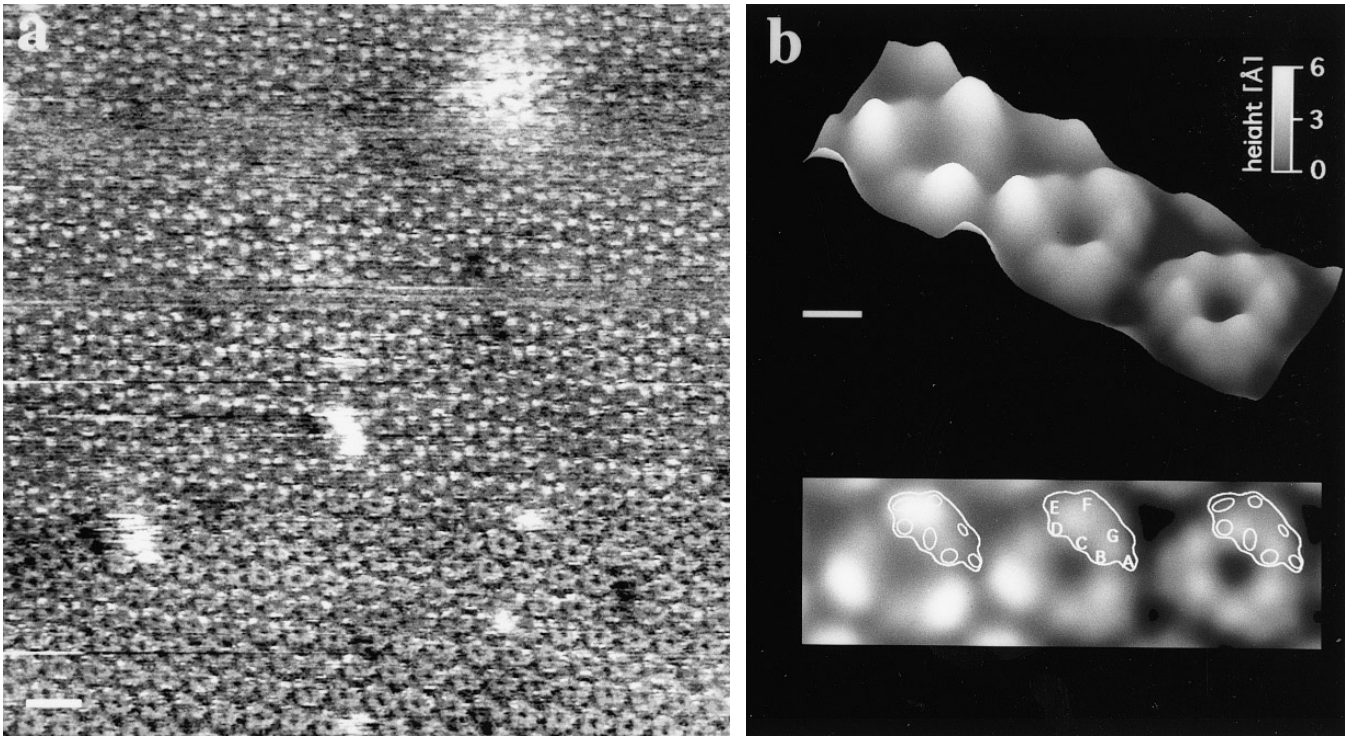

FIG. 5. Force-induced conformational change of bacteriorhodopsin. (a) The applied force of 300 pN (bottom) was decreased to 100 pN (top). (b) Correlation-averaged and threefold-symmetrized topographies of the conformational change. The middle trimer of the projection (bottom) is a computed composition of the left trimer recorded at 100 pN and the right trimer recorded at 300 pN. In the corresponding topograph, the helices derived from the atomic model of bacteriorhodopsin (Henderson *et al.*, 1990) were superimposed. On the left side, the domain corresponds to the loop connecting helices E and F. On the right side, the two prominent domains were identified as cytoplasmic loops AB and CD. Approximately 700 unit cells from three images recorded at 50–150 pN (left) and 800 unit cells from four images recorded at 300–600 pN loading force (right) were averaged, threefold symmetrized, and scaled according to the microscope parameters. To adjust the heights of these independent averages, the loops between A and B served as landmarks rather than the lipid bilayer moieties to minimize the influence of the tip geometry. Scale bars, 10 nm (a) and 2 nm (b). The full gray level range corresponds to 2 and 0.6 nm in (a) and (b), respectively.

protrusions (Figs. 4c and 4d). The force-dependent topography of bacteriorhodopsin was more distinct after conformations at corresponding forces were correlation averaged, threefold symmetrized, merged, and displayed as a relief (Fig. 5b). In comparison to the atomic model (Henderson *et al.*, 1990), the loops connecting helices A and B, and C and D, were most likely represented by the two protrusions per bacteriorhodopsin molecule when imaged at forces of 300 pN. The most prominent loop at the cytoplasmic surface, which connects helices E and F, was not visible at these forces. Imaging at approximately 100 pN, however, revealed that a prominent protrusion at the position of the E–F loop extended from the cytoplasmic bilayer surface by 0.6 nm (Müller *et al.*, 1995a).

Reversible Time-Dependent Conformational Change

The hexagonally packed intermediate layer (HPI), a typical bacterial surface layer, represents the major cell envelope protein of the radiotolerant eubacteria *Deinococcus radiodurans*. The HPI layer has been characterized biochemically (Baumeister *et al.*, 1982), by electron microscopy (Baumeister *et al.*, 1986), by atomic force microscopy (Karrasch *et al.*, 1994; Müller *et al.*, 1996a), and by scanning tunneling microscopy (Guckenberger *et al.*, 1989; Wang *et al.*, 1990; Amrein *et al.*, 1991; Stemmer *et al.*, 1991). Assembled from one protein (M_r 107 028; Peters *et al.*, 1987) forming hexamers of M_r 655 000 (Engel *et al.*, 1982), the HPI layer is a hexagonal lattice with a unit cell size of 18 nm. According to the three-dimensional model derived from electron microscopy data (Baumeister *et al.*, 1986), each hexagonal unit is composed of a massive core which encloses a pore. The protomers form spokes which emanate from the core and provide connections to adjacent units. This arrangement exhibits relatively large openings around the sixfold axes. The HPI layer is unusually resistant to chemical treatment and easy to isolate by the extraction of whole cells with detergent (Baumeister *et al.*, 1982). Little is known about the specific functions of such regular bacterial surface layers (Beveridge, 1981; Sleytr and Messner, 1983; Baumeister *et al.*, 1988). They may protect the cell from hostile factors of the environment and may serve as molecular sieves for the uptake of nutrients and release of metabolites. Further functions concern the determination of the cell shape, cell–cell recognition (Baumeister and Hegerl, 1986), and cell adhesion.

The HPI layer was extracted from whole cells (strain SARK) with lithium dodecyl sulfate and purified on a Percoll density gradient (Baumeister *et al.*, 1982). A stock solution (1 mg/ml protein) in distilled water was diluted to 20 μg/ml in 100 m*M* KCl, 20 m*M* $MgCl_2$, 10 m*M* Tris–HCl, pH 8.2, and deposited on freshly cleaved mica. After an adsorption time of 60 min at room temperature, the sample was ready to be investigated with the AFM.

The high-resolution topography of the outer HPI layer surface (Fig. 6a) clearly showed the cores and their pores. The V-shaped protrusions at the periphery of the core have been previously observed by 3D electron microscopy and by AFM (Karrasch *et al.*, 1994). Occasionally, single protomers were missing in the hexameric cores. Submolecular details became distinct after correlation averaging and sixfold symmetrization (Fig. 6b). The emanating arms connecting the cores have been resolved in the 3D structure (Baumeister *et al.*, 1986). The legs of the V-shaped units had a width of 1.06 ± 0.1 nm (Karrasch *et al.*, 1994) and the height difference to the emanating arms was 1.2 ± 0.2 nm, while the maximum height of the protrusion was 2.2 ± 0.7 nm (Müller *et al.*, 1996a).

The inner surface of the HPI layer was contoured at forces <200 pN with commercial oxide-sharpened Si_3N_4 tips (Digital Instruments Inc., Santa Barbara, CA) and carbon-deposited supertips. With both tips, time-dependent conformational changes were recorded in buffer solution (Müller *et al.*, 1996a), suggesting that the conformational change was not

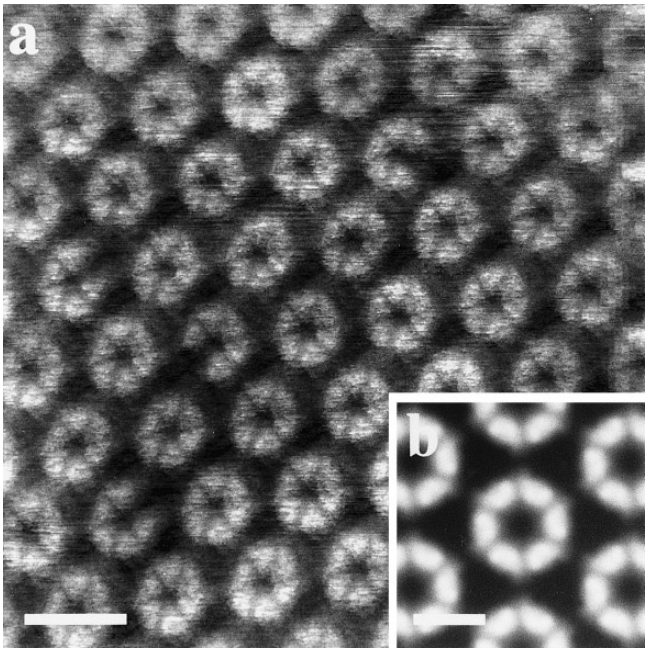

FIG. 6. Outer surface of the HPI layer. (a) High-resolution image and (b) threefold-symmetrized correlation average of the outer surface. Images were recorded in contact mode and in buffer solution. Scale bars, 20 nm (a) and 10 nm (b). The full gray level range corresponds to 5 and 2 nm in (a) and (b), respectively.

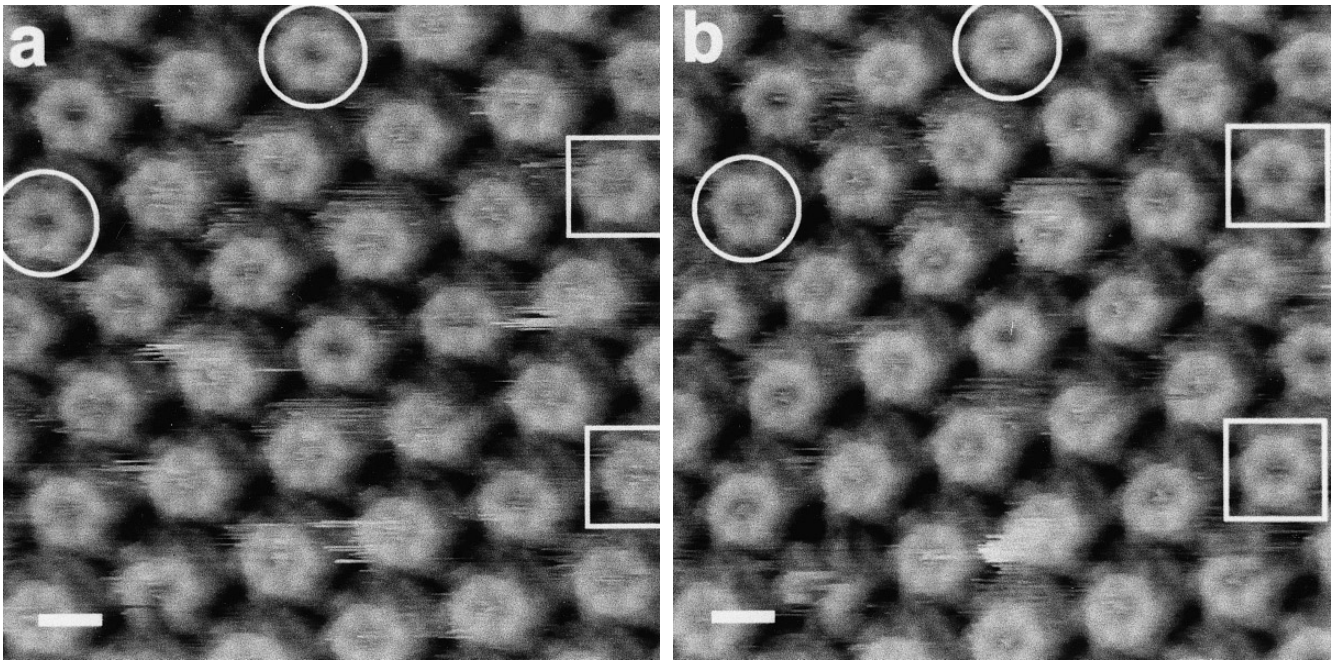

FIG. 7. Time-dependent conformational change in the inner surface of the HPI layer. (a) The protruding pores of the hexameric cores exist in two conformations in the same area: the open pore and the closed pore with a central protrusion. (a) Monitored after 5 min, some of the pores were closed (white circles), while others were now open (white squares). Images were recorded in buffer solution in contact mode at a force ≈150 pN. Scale bars, 10 nm. The full gray level range corresponds to 5 nm.

induced by specific interactions with the apex of the stylus. Figure 7a presents the submolecular details of the inner surface. The emanating arms connecting the adjacent protomers were visible before averaging. Individual pores exhibited a central depression (white circles), while others showed a single protrusion located inside the pore (white squares). When the same HPI molecules were imaged 5 min later (Fig. 7b), some of the initially open pores were closed (white circles), while some of the initially closed ones were open (white squares). The central protrusion of the closed conformation seemed to be smaller than the surrounding domains of the core.

After translational and angular alignment of the unit cells, a multivariate analysis of 330 unit cells from 10 different images was performed. The averages of the two major classes, both showing six subunits of the core and their emanating arms, exhibit either an "open" or a "closed" pore. Figure 8 displays a montage of the calculated and sixfold symmetrized topographies of both conformations. Protrusions located at the core were arranged on an equilateral hexagon of side length 4.0 ± 0.2 nm, the height difference to the emanating spokes was 2.5 ± 0.2 nm, and the maximum height of the protrusions was 2.9 ± 0.3 nm. The depression in the open conformation of the core was 1.8 ± 0.5 nm, and the depression over the protrusion of the closed conformation was 1.0 ± 0.5 nm (Müller *et al.*, 1996a).

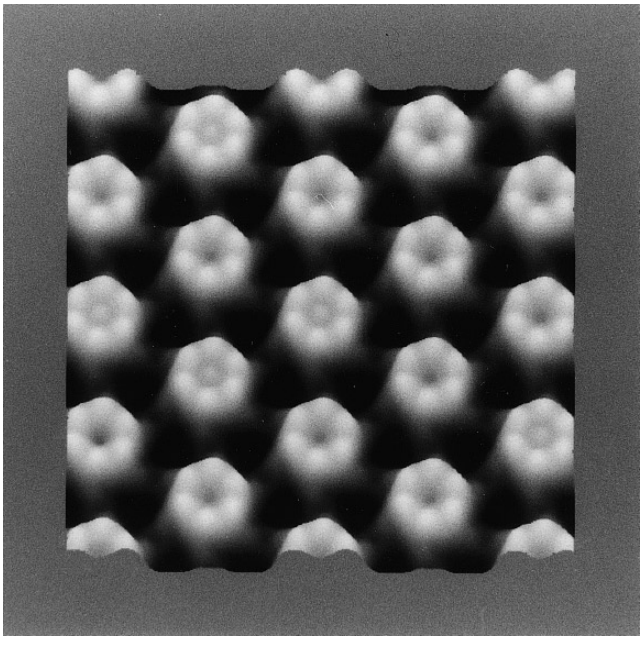

FIG. 8. Montage of the surface relief of the open and closed conformation of HPI. The correlation averages of both the open and the closed conformations were sixfold symmetrized and then assembled in the montage. The distinct arms emanating from the cores of the hexamers exhibit a counterclockwise rotation. The root mean square deviation from sixfold symmetry was 7.2%. The distance between adjacent pores is 18 nm. The full gray level range of the average corresponds to 3 nm vertical distance.

DISCUSSION

The AFM topographs of porin, bacteriorhodopsin, and the HPI layer clearly show submolecular resolution of the respective proteins. Details of the pores and the surrounding cores (porin and HPI) could be imaged without additional image processing. These high-resolution images provide evidence that the AFM fulfills the prerequisites to directly monitor function-related conformational changes of biological macromolecules.

The two topographies of the extracellular OmpF porin surface were static. Until now, it has not been possible to monitor any structural changes in the extracellular surface which could be related to the switching of the channel (Todt *et al.*, 1992; Lakey, 1987). Although energy requirements cannot be estimated from the static atomic structure (Cowan *et al.*, 1992), this finding suggested that the extracellular domains may perform a structural change (Schabert *et al.*, 1995) to vary the channel conductance.

Single loops of native bacteriorhodopsin can be imaged with the AFM at subnanometer resolution. In addition, the most prominent loop extending from the cytoplasmic surface can undergo force-induced conformational changes (Müller *et al.*, 1995a) during imaging with the AFM. This dynamic process can be repeatedly observed in a given area of the purple membrane without any detectable destruction of the surface topography. This emphasizes the sensitivity of the AFM in "touching" proteins in aqueous solution and demonstrates that biological systems must be monitored with forces less than a few hundred piconewtons to minimize sample deformation. Furthermore, biological systems require careful sample treatment; otherwise, adsorption to a support might lead to protein denaturation (Kellenberger and Kistler, 1979; Kellenberger *et al.*, 1982; Baumeister *et al.*, 1986). Nevertheless, our results suggest that it should be possible to directly monitor function-related conformational changes in bacteriorhodopsin loops such as previously detected by other methods (Steinhoff *et al.*, 1994, 1995), by AFM.

While submolecular details of the outer surface of the HPI layer have been consistently imaged in buffer solution (Karrasch *et al.*, 1993, 1994; Müller *et al.*, 1996a), two conformations, i.e., a "closed" and an "open" pore, were observed on the inner surface. These conformations were reversible and changed with time (Müller *et al.*, 1996a). Until now it has not been possible either to trigger this process while the pores were imaged with the AFM or to independently identify the functions of the HPI layer. Therefore, it is premature to draw any biologically relevant conclusions from the observed conformational change.

In summary, the results presented here demonstrate the feasibility of directly recording function-related conformational changes in native biological macromolecules with the AFM.

This work was supported by the Swiss National Foundation for Scientific Research (Grant 31-42435.94 to A.E.), the Deutsche Forschungsgemeinschaft (SFB 189 to D.J.M.), and the Maurice E. Müller Foundation of Switzerland. D.J.M. is grateful to Dr. G. Büldt for his continuous support.

REFERENCES

Amrein, M. (1989) STM on freeze-dried and Pt-Ir-C coated bacteriophage T4 polyheads, *J. Ultrastruct. Mol. Struct. Res.* **102,** 170–177.

Amrein, M., Wang, Z., and Guckenberger, R. (1991) Comparative study of a regular protein layer by scanning tunneling microscopy and transmission electron microscopy, *J. Vac. Sci. Technol.* **B9**(2), 1276–1281.

Baldwin, J. M. (1993) The probable arrangement of the helices in G protein-coupled receptors, *EMBO J.* **12,** 1693–1703.

Baumeister, W., Barth, M., Hegerl, R., Guckenberger, R., Hahn, M., and Saxton, W. O. (1986) Three-dimensional structure of the regular surface layer (HPI layer) of *Deinococcus radiodurans*, *J. Mol. Biol.* **187,** 241–253.

Baumeister, W., and Hegerl, R. (1986) Can S-layers make bacterial connexons? *FEMS microbiol. Lett.* **36,** 119–125.

Baumeister, W., Karrenberg, F., Rachel, R., Engel, A., Ten Heggeler, B., and Saxton, W. O. (1982) The major cell envelope protein of *Micrococcus radiodurans* (R1), *Eur. J. Biochem.* **125,** 535–544.

Baumeister, W., Wildhaber, I., and Engelhardt, H. (1988) Bacterial surface proteins: Some structural, functional and evolutionary aspects, *Biophys. Chem.* **29,** 39–49.

Beveridge, T. J. (1981). Ultrastructure, chemistry, and function of the bacterial wall, *Int. Rev. Cytol.* **72,** 229–317.

Binnig, G., Gerber, C., Stoll, E., Albrecht, T. R., and Quate, C. F. (1987) Atomic resolution with atomic force microscopy, *Europhys. Lett.* **3,** 1281–1286.

Binnig, G., Quate, C. F., and Gerber, C. (1986) Atomic force microscope, *Phys. Rev. Lett.* **56,** 930–933.

Binnig, G., Rohrer, H., Gerber, C., and Weibel, E. (1982) Tunneling through a controllable vacuum gap. *Appl. Phys. Lett.* **40,** 178.

Cowan, S. W., Schirmer, T., Rummel, G., Steiert, M., Ghosh, R., Pauptit, R. A., Jansonius, J. N., and Rosenbusch, J. P. (1992) Crystal structures explain functional properties of two *E. coli* porins, *Nature* **358,** 727–733.

Dencher, N. A., Dresselhaus, D., Zaccai, G., and Büldt, G. (1989) Structural changes in bacteriorhodopsin during proton translocation revealed by neutron diffraction, *Proc. Natl. Acad. Sci. USA* **86,** 7876–7879.

Drake, B., Prater, C. B., Weisenhorn, A. L., Gould, S. A. C., Albrecht, T. R., Quate, C. F., Cannell, D. S., Hansma, H. G., and Hansma, P. K. (1989) Imaging crystals, polymers, and processes in water with the atomic force microscope, *Science* **243,** 1586–1588.

Engel, A., Baumeister, W., and Saxton, W. (1982) Mass mapping of a protein complex with the scanning transmission electron microscope, *Proc. Natl. Acad. Sci. USA* **79,** 4050–4054.

Grigorieff, N., Ceska, T. A., Downing, K. H., Baldwin, J. M., and Henderson, R. (1996) Electron-crystallographic refinement of the structure of bacteriorhodopsin, *J. Mol. Biol.* **259,** 393–421.

Guckenberger, R., Heim, M., Cevc, G., Knapp, H. F., Wiegräbe, W., and Hillebrand, A. (1994) Scanning tunneling microscopy of insulators and biological specimens based on lateral conductivity of ultrathin water films, *Science* **266,** 1538–1540.

Guckenberger, R., Wiegräbe, W., Hillebrand, A., Hartman, T.,

Wang, Z., and Baumeister, W. (1989) Scanning tunneling microscopy of a hydrated bacterial surface protein, *Ultramicroscopy* **31,** 327–332.

Havelka, W. A., Henderson, R., Heymann, J. A. W., and Oesterhelt, D. (1993) Projection structure of halorhodopsin from *Halobacterium halobium* at 6 Å resolution obtained by electron cryo-microscopy, *J. Mol. Biol.* **234,** 837–846.

Henderson, R., Baldwin, J. M., Ceska, T. A., Zemlin, F., Beckman, E., and Downing, K. H. (1990) Model for the structure of bacteriorhodopsin based on high-resolution electron cryo-microscopy, *J. Mol. Biol.* **213,** 899–929.

Henderson, R., Jubb, J. S., and Whytock, S. (1978) Specific labelling of the protein and lipid on the extracellular surface of purple membrane, *J. Mol. Biol.* **123,** 259–274.

Hoenger, A., Ghosh, R., Schoenenberger, C.-A., Aebi, U., and Engel, A. (1993) Direct *in situ* structural analysis of recombinant outer membrane proteins expressed in an OmpA-deficient mutant *Escherichia coli* strain, *J. Struct. Biol.* **111,** 212–221.

Hoh, J. H., Lal, R., John, S. A., Revel, J.-P., and Arnsdorf, M. F. (1991) Atomic force microscopy and dissection of gap junctions, *Science* **253,** 1405–1408.

Hoh, J. H., Sosinsky, G. E., Revel, J.-P., and Hansma, P. K. (1993) Structure of the extracellular surface of the gap junction by atomic force microscopy, *Biophys. J.* **65,** 149–163.

Jap, B. K., Zulauf, M., Scheybani, T., Hefti, A., Baumeister, W., Aebi, U., and Engel, A. (1992) 2D crystallization: from art to science, *Ultramicroscopy* **46,** 45–84.

Jubb, J. S., Worcester, D. L., Crespi, H. L., and Zaccai, G. (1984) Retinal location in purple membrane of *Halobacterium halobium:* A neutron diffraction study of membranes labeled *in vivo* with deuterated retinal, *EMBO J.* **3,** 1455–1461.

Karrasch, S., Dolder, M., Hoh, J., Schabert, F., Ramsden, J., and Engel, A. (1993) Covalent binding of biological samples to solid supports for scanning probe microscopy in buffer solution, *Biophys. J.* **65,** 2437–2446.

Karrasch, S., Hegerl, R., Hoh, J., Baumeister, W., and Engel, A. (1994) Atomic force microscopy produces faithful high-resolution images of protein surfaces in an aqueous environment, *Proc. Natl. Acad. Sci. USA* **91,** 836–838.

Kates, M., Kushawa, S. C., and Sprott, G. D. (1982) Lipids of purple membrane from extreme halophiles and of methanogenic bacteria, *Methods Enzymol.* **88,** 98–111.

Kellenberger, E., Häner, M., and Wurtz, M. (1982) The wrapping phenomenon in airdried and negatively stained preparations, *Ultramicroscopy* **9,** 139–150.

Kellenberger, E., and Kistler, J. (1979) The physics of specimen preparation, in Mason, W. H. R. (Ed.), Advances in Structure Research by Diffraction Methods, pp. 49–79, Vieweg, Wiesbaden.

Knapp, H. F., Wyss, R., Häring, R., Henn, C., Guckenberger, R., and Engel, A. (1995) Hybrid scanning transmission electron/scanning tunneling microscope for the preparation and investigation of biomolecules, *J. Microsc.* **177,** 31–42.

Lakey, J. H. (1987) Voltage gating in porin channels, *FEBS Lett.* **211,** 1–4.

Maaloum, M., Chretien, D., Karsenti, E., and Hörber, J. K. H. (1994) Approaching microtubule structure with the scanning tunneling microscope (STM), *J. Cell Sci.* **107,** 3127–3131.

Mou, J., Czajkowsky, D. M., Sheng, S., Ho, R., and Shao, Z. (1996) High resolution surface structure of *E. coli* GroES oligomer by atomic force microscopy, *FEBS Lett.* **381,** 161–164.

Müller, D. J., Baumeister, W., and Engel, A. (1996a) Conformational change of the hexagonally packed intermediate layer imaged by atomic force microscopy, *J. Bacteriol.* **178,** 3025–3030.

Müller, D. J., Büldt, G., and Engel, A. (1995a) Force-induced conformational change of bacteriorhodopsin, *J. Mol. Biol.* **249,** 239–243.

Müller, D. J., Schabert, F. A., Büldt, G., and Engel, A. (1995b) Imaging purple membranes in aqueous solutions at subnanometer resolution by atomic force microscopy, *Biophys. J.* **68,** 1681–1686.

Müller, D. J., Schoenenberger, C. A., Büldt, G., and Engel, A. (1996b) Immuno-atomic force microscopy of purple membrane, *Biophys. J.* **70,** 1796–1802.

Oesterhelt, D., and Stoeckenius, W. (1974) Isolation of the cell membrane of *Halobacterium halobium* and its fraction into red and purple membrane, *Methods Enzymol.* **31,** 667–678.

Ohnesorge, F., and Binnig, G. (1993) True atomic resolution by atomic force microscopy through repulsive and attractive forces, *Science* **260,** 1451–1456.

Peters, J., Peters, M., Lottspeich, F., Schäfer, W., and Baumeister, W. (1987) Nucleotide sequence of the gene encoding the *Deinococcus radiodurans* surface protein, derived amino acid sequence, and complementary protein chemical studies, *J. Bacteriol.* **169,** 5216–5223.

Rosenbusch, P. (1974) Characterization of the major envelope protein from *Escherichia coli, J. Biol. Chem.* **249,** 8019–8029.

Schabert, F. A., and Engel, A. (1994) Reproducible acquisition of *Escherichia coli* porin surface topographs by atomic force microscopy, *Biophys. J.* **67,** 2394–2403.

Schabert, F. A., Henn, C., and Engel, A. (1995) Native *Escherichia coli* OmpF porin surfaces probed by atomic force microscopy, *Science* **268,** 92–94.

Schertler, G. F. X., Villa, C., and Henderson, R. (1993) Projection structure of rhodopsin, *Nature* **362,** 770–773.

Schulz, G. (1993) Bacterial porins: Structure and function, *Curr. Opin. Cell Biol.* **5,** 701–707.

Sleytr, U. B., and Messner, P. (1983) Crystalline surface layers on bacteria, *Annu. Rev. Microbiol.* **37,** 311–339.

Sonnenfeld, R., and Hansma, P. K. (1986) Atomic resolution microscopy in water, *Science* **232,** 211–213.

Steinhoff, H.-J., Mollaaghababa, R., Altenbach, C., Hideg, K., Khorana, H. G., and Hubbell, W. L. (1994) Time-resolved detection of structural changes during the photocycle of spin-labeled bacteriorhodopsin, *Science* **266,** 105–107.

Steinhoff, H.-J., Mollaaghababa, R., Altenbach, C., Khorana, H. G., and Hubbell, W. L. (1995) Site directed spin labeling studies of structure and dynamics in bacteriorhodopsin, *Biophys. Chem.* **56,** 89–94.

Stemmer, A., Reichelt, R., Wyss, R., and Engel, A. (1991) Biological structures imaged in a hybrid scanning transmission electron microscope and scanning tunneling microscope, *Ultramicroscopy* **35,** 255–264.

Subramaniam, S., Gerstein, M., Oesterhelt, D., and Henderson, R. (1993) Electron diffraction analysis of structural changes in the photocycle of bacteriorhodopsin, *EMBO J.* **12,** 1–8.

Todt, J. C., Rocque, W. J., and McGroarty, E. J. (1992) Effects of pH on bacterial porin function, *Biochem.* **31,** 10471–10478.

Wang, Z., Hartman, T., Baumeister, W., and Guckenberger, R. (1990) Thickness determination of biological samples with a z-calibrated scanning tunneling microscope, *Proc. Natl. Acad. Sci. USA* **87,** 9343–9347.

Yang, J., Tamm, L. K., Tillack, T. W., and Shao, Z. (1993) New approach for atomic force microscopy of membrane proteins, *J. Mol. Biol.* **229,** 286–290.